APPARATUS AND DEMONSTRATION NOTES

Jeffrey S. Dunham, *Editor*
Department of Physics, Middlebury College, Middlebury, Vermont 05753

This department welcomes brief communications reporting new demonstrations, laboratory equipment, techniques, or materials of interest to teachers of physics. Notes on new applications of older apparatus, measurements supplementing data supplied by manufacturers, information which, while not new, is not generally known, procurement information, and news about apparatus under development may be suitable for publication in this section. Neither the *American Journal of Physics* nor the Editors assume responsibility for the correctness of the information presented. Submit materials to Jeffrey S. Dunham, *Editor.*

A course in computer-based data acquisition

W. N. Hubin[a)]
Department of Physics, Kent State University, Kent, Ohio 44242

(Received 25 February 2000; accepted 15 August 2001)

The evolution of a course in computer-based data acquisition and analysis is described. The physics of the sensors, the physics of the system under study, and practical electrical measurement techniques are emphasized in this course, as well as computer hardware and software. Three experiments of particular physical interest are described in detail: heat flow in a metal plate, light-emitting diode characteristics, and the sounds generated by a speech chip.
[DOI: 10.1119/1.1410951]

I. INTRODUCTION

Past contributors to this journal have described various approaches to a computer-based data acquisition course. Nine years ago, Kocher[1] described a course that built on preceding analog and digital electronics courses and used the IBM PC-AT and its serial/parallel input/output board with QuickBASIC as the programming language; the experiments emphasized digital-to-analog (D/A) and analog-to-digital (A/D) conversions at the chip level. Eight years ago, Maps[2] described a course using an 80386-based PC with commercially available data acquisition boards and commercial data acquisition software (ASYST). In this article we describe (a) the evolution of our data acquisition/analysis course over a period of 20 years and (b) three experiments which are of potential interest for traditional student physics laboratories as well as for teaching data acquisition techniques.

II. COURSE EVOLUTION

Since 1980 the Department of Physics at Kent State University has offered a course intended to teach students how to choose, set up, and utilize a computer in the physics laboratory for data acquisition, analysis, and presentation. This is in contrast with the usual student laboratory experiment where a pre-existing computer with pre-existing sensors and software is simply used by the student. Our course doesn't require a digital electronics background and so is available to technology, computer science, and chemistry students, but some prior experience in computer programming is expected. However, in the last few years, because of the general decline in programming skills, the computer prerequisite has been interpreted to mean that an ability to navigate through modern Windows point-and-click program is expected. Many opportunities exist to discuss the physics of the types of sensors that are available (temperature, force/acceleration, radiation) and the practical electrical problems (electronic/thermal noise, ground loops, amplification, aliasing) encountered in using them.

The course is a requirement (at the senior level) for all students who choose the computer hardware option in our undergraduate major; it is also available to graduate students. The course began in 1980 when an equipment grant for an LSI-11 (PDP-11) minicomputer system was received. At that time there was no data acquisition software available for this system and therefore assembly language had to be taught before application programs could be written.

In 1984 the author began teaching the course and, within a few years, it had become obvious that the personal computer (PC), in conjunction with plug-in boards, had replaced the minicomputer in the science and engineering laboratory, at least for most small laboratories. In 1989 the author received an equipment grant that provided a (then) state-of-the-art 80386-based PC with a Metrabyte (now Keithley Metrabyte) data acquisition card (eight differential channels, 12-bit A/D converter). Supporting software with this board included routines that could be called from the QuickBASIC high-level language so that meaningful physics measurements could begin much earlier in the course. The textbook used[3] was a very useful manual, written specifically for the IBM PC, and dealt with important aspects of sources of noise, signal conditioning, and software analysis, as well as the BASIC approach to data acquisition (BASIC affords direct access to the PC's separate input/output address space through the OUT and INP statements).

Since that time, of course, the amount of hardware and software intended for laboratory use with PCs has increased

by orders of magnitude. Many vendors vie for an instructor's full attention. However, the approach taken in the computer part of this course has always been to expose students to a wide range of software and hardware options, from the simple and inexpensive (and time-intensive) to the integrated, complex, and expensive.

The very cheapest methods are (a) using the parallel, serial or game ports with one's own hardware circuits and (b) buying a bare plug-in board and populating it with integrated circuits, and then writing one's own acquisition software. These are still practical approaches for low rates of data acquisition and literature exists[4–13] to get the new user started. (Eventually, new PCs are expected to eliminate internal slots and the parallel and serial ports in favor of the Universal Serial Bus.)

Our experiments begin by using QuickBASIC programs that call subroutines from the library provided by the manufacturer of the Metrabyte board. Acquired data are analyzed and graphed with the help of scientific software (SigmaPlot). This low-cost DOS approach is still viable because QBASIC is provided with the Windows operating system. An example of an interesting heat-flow experiment that uses data acquired and analyzed in this fashion is described in Sec. III below.

The next higher level of integration is achieved through the use of software such as National Instruments LabWindows©, which assists the user in generating a traditional high-level program (with click-down subroutine calls for combined data acquisition, analysis, graphing, and real-time checks). This approach has been used to obtain audio data from a speech chip and to generate the frequency spectrum, as described in Sec. V below. Initially LabWindows supported both the QuickBASIC and C programming languages; now only C is supported.

More recent data acquisition boards typically come with some supporting Windows-based software, thus allowing the user to configure the board (choosing which channels to use and adjusting the polarity and gain of the amplifier for the A/D converter) in software as well as displaying the data graphically immediately after obtaining it—a great help in checking the quality of the data.

The most popular (and most expensive) software now available offers integrated data collection, analysis, and presentation through what the vendors describe as ''graphical'' programming. This involves constructing a program by graphically patching together, in flowchart form, symbols that represent the flow of information from input to analysis to presentation output. A long program can challenge the available screen ''real estate!'' Even though the result of graphical programming is a C language program, the user almost never has to peer below this graphical level. The two most popular graphical programming languages are National Instruments LabView© and Hewlett–Packard's HPVee©. Even though these languages are growing in popularity,[14] they are proprietary and quite expensive, so the course only presents an introduction to them.

Handouts from the current data acquisition literature are used to introduce students to the physics of sensors and electrical considerations as well as trends in hardware and software. In this course we have observed the decline of DOS and the gradual ascension of Windows as the preferred software platform; the 20-Mbyte hard drive and 64-kbyte segmented memory space have evolved into gigabyte hard drives and 128-Mbyte memory; also, the processor has evolved from a 4.77-MHz 16-bit processor to a 1-GHz 32-bit processor. Throughout, the goal in this course has been to provide students with enough background so that, in the future, they can intelligently choose appropriate software and hardware for a given experimental problem.

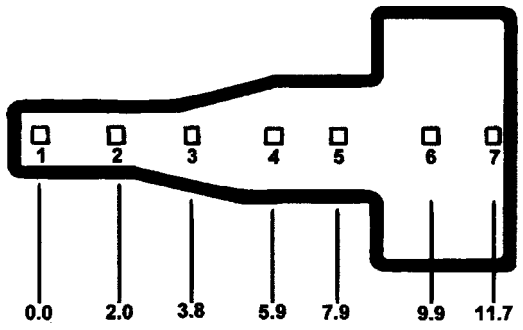

Fig. 1. A 1/8-in.-thick aluminum plate with seven solid-state temperature sensors is used to study statistical errors and heat flow. The numbers are the locations in centimeters of the sensors, relative to the left-most sensor.

Many of the undergraduate students taking this course have found it to be one of the most immediately valuable courses they have taken because of the intensive use of computer-based data acquisition in industry and because ''competing'' graduates will most likely not have this background. Graduate students in physics mostly prefer to sit in on the lecture part or learn the data acquisition in use from their predecessors when they begin their experimental research. But graduate students in computer science and technology have always formed a significant percentage of the enrollment. The course is a continuing challenge for the instructor, both for the daily demands of maintaining the hardware and software and assisting students and for keeping abreast of this rapidly advancing field.

For physics instructors at other schools and universities, whether they wish to offer such a course or not, some of the experiments we do are physically interesting and emphasize the experimental advantages and gains made possible by connecting sensors directly to computers, and thus lend

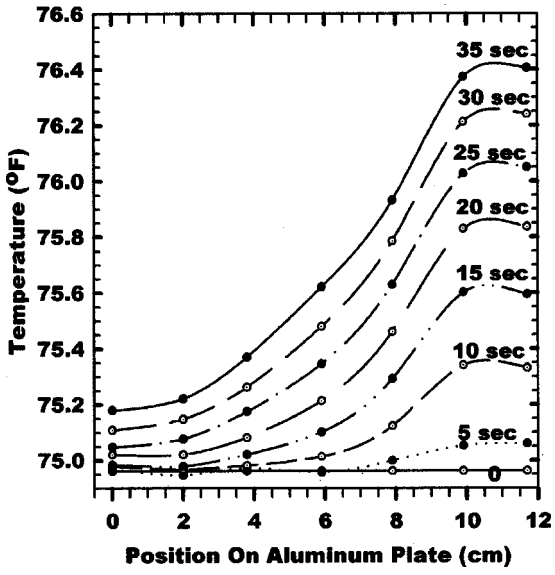

Fig. 2. Temperature as a function of time along the aluminum plate, while being heated by a warm hand between sensor six and seven.

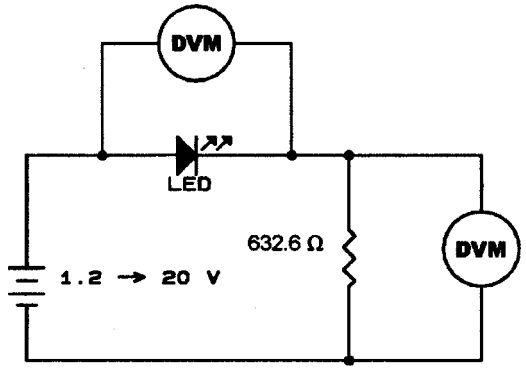

Fig. 3. Circuit for measuring LED current–voltage characteristics (with manual adjustment of LED current), using a standard laboratory powered breadboard.

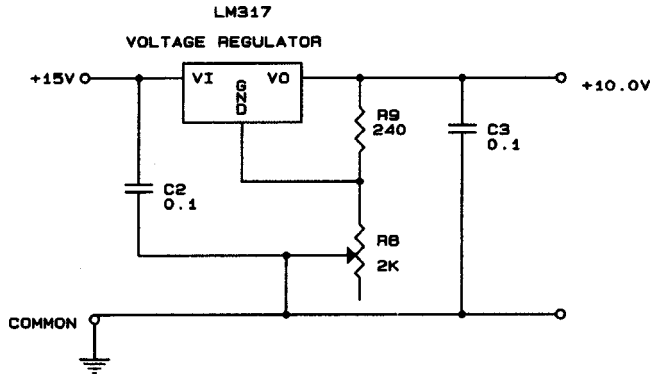

Fig. 5. Regulated 10-V supply for the circuit of Fig. 4.

themselves to use in the more traditional physics laboratory courses where the emphasis is just on the physics.

III. HEAT FLOW IN A METAL PLATE

One of the first experiments we do involves measuring the changes in the temperature of a metal plate, initially at room temperature, as a function of time and location, when we place a warming hand on it. This experiment serves to introduce (a) the use of averaging to reduce noise, (b) sensor calibration considerations, and (c) an example of how new insights into common physical phenomena are made possible by computer-based data acquisition.

I have epoxied seven solid-state temperature sensors to a small aluminum plate (Fig. 1). The inexpensive sensors are the LM34DZ from National Semiconductor. They require a 5-V supply and their output varies linearly from 0 V at 0 °F to 1.0 V at 100 °F with a ''typical'' accuracy of ±1 °F. (A Celsius version is available as the LM35DZ.) The sensors are connected directly to seven of the eight multiplexed (differential) inputs of the 12-bit A/D converter on the MetraByte board. We first take 100 or more measurements of the output from one sensor in order to determine the amount of electrical noise/thermal fluctuations present under ambient conditions. For these inexpensive sensors, the standard deviation from the mean is typically 0.5 mV or 0.05 °F.

Second, the average voltage (and temperature) from each sensor is compared with the overall average for all seven sensors and (for lack of a more accurate, calibrated thermometer) this overall average, subtracted from an individual average, is used later as a correction factor for that sensor, in recognition of the fact that all the sensors are initially at the same temperature, and we are only interested in changes in temperature.

After discussing and analyzing the fluctuations in sensor outputs and their different calibrations, an experimental run consists of obtaining 100 temperature readings from each sensor every 5 or 6 s, for an elapsed time of 35 or 42 s. Heat is applied after the first measurements are made, so these data can be used to calibrate the sensors to their average value while they are still at the same temperature. Figure 2 presents a typical graph of analyzed data, showing the variation of temperature with both time and location on the plate. For these data the warming hand was placed between sensors six and seven (1.8 cm apart). Notice the very good temperature resolution, for a maximum temperature gain of only 1.5 °F.

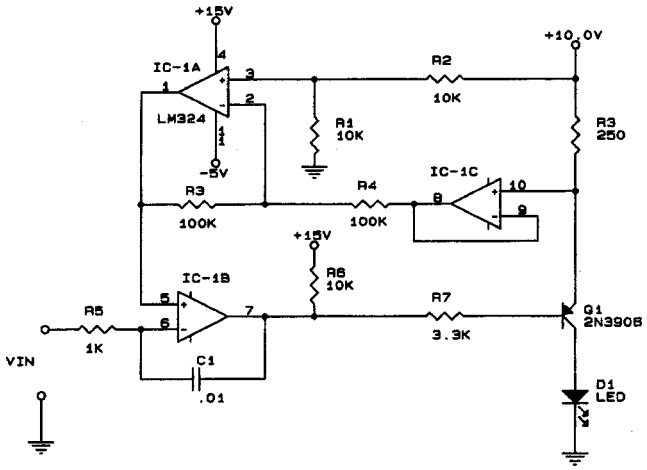

Fig. 4. Programmable current generator circuit for automatically measuring LED current–voltage characteristics. A D/A converter is used to control the LED current and an A/D converter is used to measure the LED voltage.

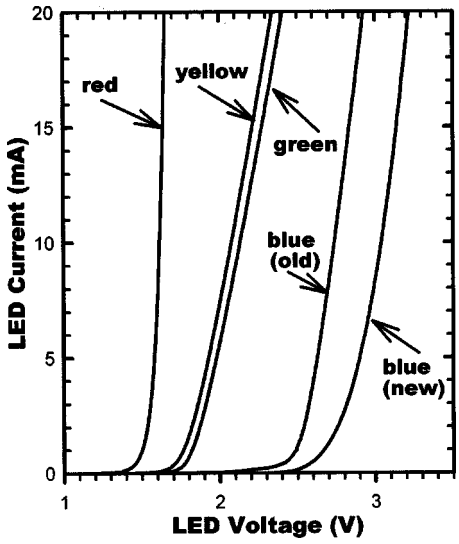

Fig. 6. Dynamic resistance characteristics of five LEDs, measured with the circuit of Fig. 4.

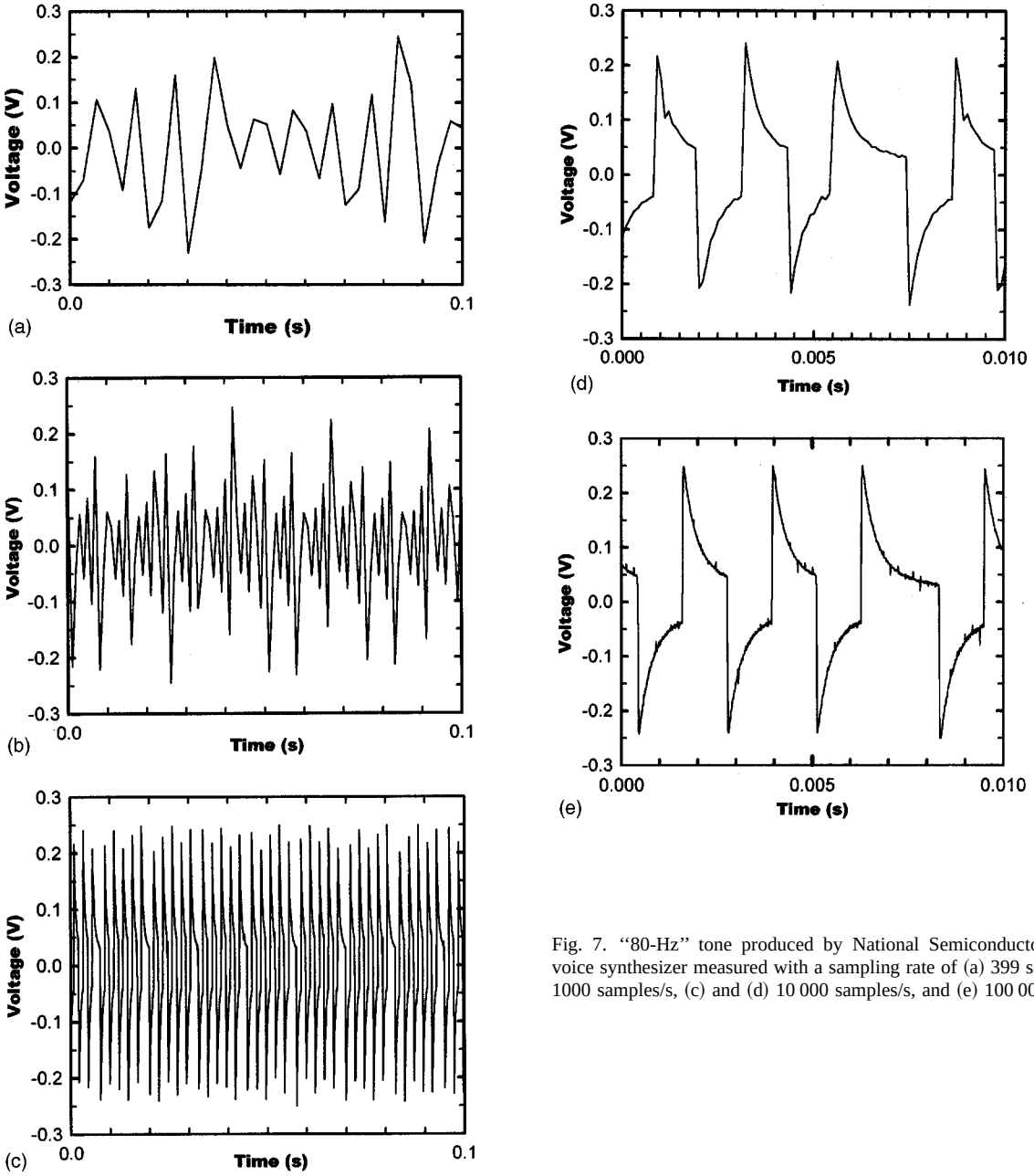

Fig. 7. "80-Hz" tone produced by National Semiconductor Digitalker voice synthesizer measured with a sampling rate of (a) 399 samples/s, (b) 1000 samples/s, (c) and (d) 10 000 samples/s, and (e) 100 000 samples/s.

IV. LIGHT-EMITTING DIODE CURRENT–VOLTAGE CHARACTERISTICS

Light-emitting diodes (LEDs) are interesting for the physics behind their light production (including the variation of turn-on voltage with wavelength) as well as for the practical consequences of their nonlinear resistance. They can therefore be used to provide a good introduction to measuring both dependent and independent parameters in a physical system. Also, a LED's $I-V$ curve is required for precise calculations of the current-limiting resistor required in any actual circuit. (More qualitatively, Walkiewicz and Kirk have shown that $I-V$ curves for LEDs are readily generated on an oscilloscope.[15])

Each student is required to characterize at least two different LEDs. Typically this experiment has served to introduce the use of IEE-488/HP-IB/GPIB instruments as well. Using the circuit shown in Fig. 3, the student first adjusts the voltage to obtain a LED current of 20 mA and then reduces the exciting voltage carefully in steps. Initially the steps are best chosen by reference to the current (as measured by the voltage across the precision 632.6-Ω resistor); at the knee of the curve it is better to use the voltage across the LED. The resistance of the precision resistor is large enough to help protect the LED from excessive currents while small enough to minimize the voltmeter current (less than 0.01% with a voltmeter input impedance of 11 MΩ).

Another recently devised circuit (Figs. 4 and 5) has been used to automate the entire process, taking thousands of data points in a few seconds. This is a voltage-controlled current generator circuit. The applied control voltage (from the data acquisition board's D/A converter) generates a nearly proportional LED current, independently of the type of LED. (The proportionality constant varies smoothly from 3.96 V/mA of current at 1.0 mA to 4.01 V/mA of current at 20.0 mA.)

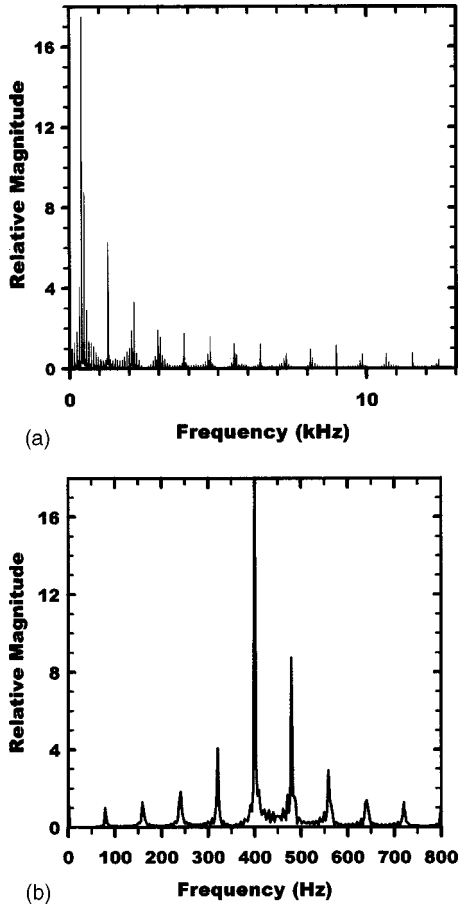

Fig. 8. Fast Fourier transform of the ''80-Hz'' tone produced by National Semiconductor Digitalker voice synthesizer; sampling rate of 100 000 samples/s. (a) Full spectrum. (b) Fundamental and lower harmonics.

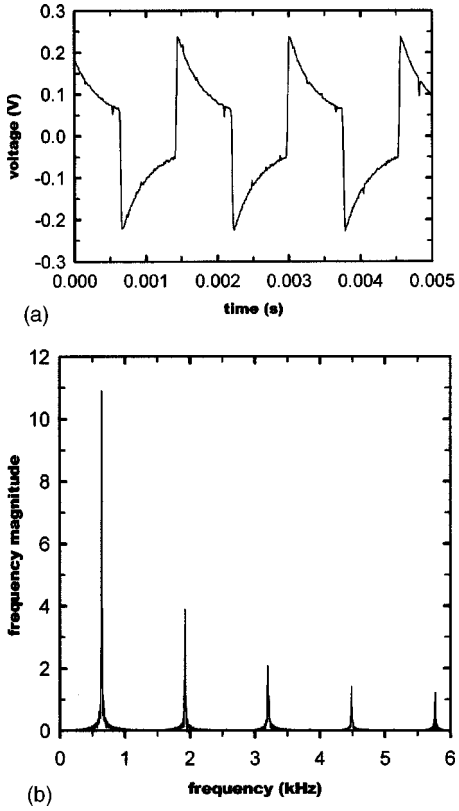

Fig. 9. ''400-Hz'' tone produced by National Semiconductor Digitalker voice synthesizer with a sampling rate of 80 645 samples/s: (a) the voltage waveform. (b) fast Fourier transform.

In this circuit, for a control voltage between 0 and 5.0 V, the LED current varies from 0 to a maximum given by the relationship

$$I_{\max} = V_{\text{ref}}/(2R),$$

where R is the resistance of resistor R3 and V_{ref} is the voltage at the junction of resistors R2 and R3. Because our circuit uses a regulated $+10.0$-V supply for V_{ref}, our maximum current is $10.0\,\text{V}/(2\times 250\,\Omega) = 0.020\,\text{A} = 20\,\text{mA}$.

Figure 6 shows the $I-V$ characteristics for five different LEDs determined using this circuit. The curve for ''blue (old)'' is for one of the earliest blue LEDs; its threshold voltage is significantly less than that for a new generation blue LED, ''blue (new),'' as well as being much less bright.

V. OUTPUT VOLTAGE AND FREQUENCY SPECTRUM GENERATED BY A DIGITAL SPEECH SYNTHESIZER

Another system of intrinsic interest is a sound generator. It affords an opportunity for discovering the misinformation obtained (aliasing) when the sampling frequency is less than twice the highest frequency present in the source (Nyquist criterion). A standard signal generator could be used for this kind of experiment, but it is far more interesting to use a speech chip which can produce any harmonic-rich sound. The speech processor chip I use is based on a 4.0-MHz frequency generator circuit, so many frequencies can be expected to be present.

National Semiconductor's DIGITALKER™ DT1050 speech synthesizer kit (available from Jameco Electronics[16]) provides for a circuit that generates 137 separate words, or parts of words, as well as two different tones (listed by the manufacturer as an 80-Hz tone and a 400-Hz tone). The application notes for the chip set include a bandpass filter circuit to produce maximum frequency response. I use this circuit except with an added 10-kΩ volume control just before the specified LM386 audio amplifier. The input voltage to this volume control is measured by the A/D converter in the PC; it has a variation of about ± 0.3 V and therefore no additional amplification will be required for many data acquisition boards.

I normally provide students with measurements I have made of the ''80-Hz'' tone and let them do all their work with the ''400-Hz'' tone. If the ''80-Hz'' tone exhibited a purely sinusoidal variation with time, the Nyquist criterion tells us that a sampling rate of twice that value (160 samples/s) is the minimum required to verify the stated frequency. However, the actual voltage output from the circuit sampled at a rate of 399 samples/s shows us that many higher frequencies are present [Fig. 7(a)].

Fortunately, we can easily increase the sampling rate until we see no change. A sampling rate of 1000 samples/s, Fig. 7(b), is still much too low. At 10 000 samples/s [Figs. 7(c) and 7(d)], the basic waveform emerges, but obviously there are still some unresolved higher frequencies. At the highest available sampling rate of 100 000 samples/s [Fig. 7(e)], all

of the overtones appeared to be resolved. This provides students with a good idea of what to expect when they make measurements of the ''400-Hz'' tone, and emphasizes the importance of an adequately high sampling rate when measuring a complex waveform.

Of course, we can now estimate the fundamental frequency of this ''80-Hz'' tone. From Fig. 7(e), the first two cycles required nearly 0.005 s and so that the frequency is $f=1/T=1/0.0025\,\mathrm{s}=400\,\mathrm{Hz}$. However, there is a longer time between the third and fourth cycles and this represents a low frequency modulation that occurs every five cycles [Fig. 7(c)] and this allows us to estimate a (very weak) fundamental frequency of $400\,\mathrm{Hz}/5=80\,\mathrm{Hz}$, just as the manufacturer claims. (The bandpass circuit preceding our voltage measurement presumably reduces the amplitude of this fundamental.)

Some students will admit to having heard of the fast Fourier transform (FFT) but none has ever admitted to using it. This experiment is a perfect opportunity. Figure 8(a) shows the frequency spectrum up to 13 kHz; Fig. 8(b), at lower frequencies, shows clearly that the fundamental frequency is in fact 80 Hz because all other frequencies present are the possible odd and even overtones of 80 Hz.

When students make their measurements and do their analysis of the ''400-Hz'' tone, they expect a similar situation to prevail. It does *not*—in two interesting ways—but I always let the students discover that for themselves! Figure 9(a) is the voltage output for this ''400-Hz'' tone; the lowest frequency appears to be about $f=1/T=1/0.001\,56\,\mathrm{s}\approx 640\,\mathrm{Hz}$. The FFT [Fig. 9(b)] confirms the fact that this fundamental frequency is exactly 640 Hz (2^3 greater than the ''80 Hz'') and that in this instance only the *odd* harmonics are present!

In recent years wavelet analysis has joined the fast Fourier transform as a tool for studying periodic phenomena.[17,18] For example, wavelets are being used to compress fingerprint information. In general, it can be said that wavelet analysis is better than FFT analysis when a signal is changing rapidly—as in the pressure waves generated by speech. When wavelet software becomes more affordable, the building-block parts of words that are produced by this speech chip should lend themselves to study with this newer analysis tool.

ACKNOWLEDGMENTS

The purchase of the first PC and data acquisition board for this course was made possible through NSF Instrumentation and Laboratory Improvement Program Grant No. PHY-8851629. The programmable current generator circuit shown in Fig. 4 was designed by Alan Baldwin.

[a]Electronic mail: hubin@physics.kent.edu

[1]J. Maps, ''A computer-based data acquisition laboratory for undergraduates,'' Am. J. Phys. **61**, 651–655 (1993).

[2]Carl A. Kocher, ''A laboratory course in computer interfacing and instrumentation,'' Am. J. Phys. **60**, 246–251 (1992).

[3]Stephen C. Gates with Jordan Becker, *Laboratory Automation Using the IBM PC* (Prentice–Hall, Englewood Cliffs, NJ, 1989).

[4]Dhananjhay V. Gadre, *Programming the Parallel Port: Interfacing the PC for Data Acquisition and Process Control* (R&D Books, Lawrence, KS, 1998).

[5]Jan Axelson, *Parallel Port Complete: Programming, Interfacing, & Using the PC's Parallel Printer Port* (Lakeview Research, Madison, WI, 1996).

[6]Jan Axelson, *Serial Port Complete: Programming and Circuits for RS-232 and RS-485 Links and Networks* (Lakeview Research, Madison, WI, 1999).

[7]Kevin R. Hoskins, ''Add Analog I/O Channels to a Serial Port,'' Test Meas. World **17**, 29–33 (September, 1997). Program code is in C; 12-bit resolution, 3300 samples/s.

[8]Jerry Steele, ''Interface 12-Bit ADCs to Laptops or PCs,'' Electron. Des. **43**, 89–92 (October, 1995). Three circuits are given; high speed can be achieved by using a cache memory IC next to the A/D converter.

[9]John S. Jacono, ''Programming Serial Ports,'' Pop. Electron. **10**, 63–87 (August, 1993).

[10]Bruce Thomas, ''Inexpensive parallel-port interface controls power-strip outlets,'' Personal Eng. Instrum. News **10**, 50–55 (October, 1993).

[11]Alexander Eisen, ''Data Acquisition Made Easy,'' Electron. Des. **44**, 111–112 (May, 1996). Program code is in C; 12-bit resolution, sampling to 100 000/s.

[12]Clayton B. Grantham, ''Capture Fast Analog Signals with Your PC's Printer Port,'' Test Meas. World **16**, 9–14 (December, 1996). Uses a 2k external memory IC to achieve 16-bit resolution at 100 000 samples/s, with output to a spreadsheet.

[13]Ed Ramsden, ''A Do-It-Yourself Data Acquisition Card,'' Sens. Data Acquisition **15**, 26–32 (1998).

[14]Ed Baroth, Chris Hartsough, Amy Holst, and George Wells, ''An Evaluation of LabVIEW 5.0 and HP VEE 5.0,'' Evaluation Eng. **38**, 64–75 (April, 1999).

[15]Thomas A. Walkiewicz and James R. Kirk, ''Characteristic Curves,'' Phys. Teach. **32**, 90–92 (1994).

[16]Jameco, 1355 Shoreway Road, Belmont, CA 94002-4100.

[17]Gilbert Strang, ''Wavelets,'' Am. Sci. **82**, 250–255 (May–June, 1994).

[18]Matt Perry, ''Wavelets help resolve uncertainties associated with FFTs,'' Personal Eng. **12**, 50–53 (March, 1995).

Investigating vortical dipolar flows using particle image velocimetry: An experiment for the advanced undergraduate laboratory

Yakov Afanasyev[a)]
Department of Physics and Physical Oceanography, Memorial University of Newfoundland, St. John's, Newfoundland A1B 3X7, Canada

(Received 8 May 2001; accepted 15 August 2001)

This paper describes a laboratory experiment designed to study vortex dipoles, fascinating structures that occur in geophysical and industrial turbulent flows. A particle image velocimetry measurement system is used to measure the velocity and vorticity fields in the flow. The apparatus required for the experiment is inexpensive and easy to construct. © *2002 American Association of Physics Teachers.*
[DOI: 10.1119/1.1410952]

I. INTRODUCTION

A vortex dipole is a jet flow with a system of two vortices of opposite sign at its front. Vortex dipoles are fundamental elements of complex chaotic flows usually denoted by the term ''two-dimensional turbulence'' and occur in the ocean, the atmosphere, and in industrial processes.[1] These structures are a fascinating subject of current research in geophysical fluid dynamics. Figure 1 shows a typical example of a vortex dipole as observed in a satellite image of the ocean surface temperature.[2] The dipole is formed by cold water shown as a darker color in the image. Although these flows are described in general by nonlinear equations of motion which are not easy to analyze, their global properties can be described using the conservation laws for mass and linear momentum. Simply put, the dynamics of these structures can be understood from straightforward application of Newton's second law of motion. This makes vortex dipoles an attractive subject for study in an undergraduate experiment. The goal of this paper is to describe a simple, low-cost experiment for the advanced undergraduate laboratory.

Vortex dipoles translate through the fluid and can therefore be characterized by their net linear momentum. This means that the action of a force is required to generate the dipoles. In the ocean the wind can often apply such a localized force on the ocean surface. Another condition is essential for the generation of dipoles: The flow must be planar. Dipoles readily occur in a density stratified (layered) fluid where the gravitational force suppresses vertical motion. To make the flow visible some indicator (passive tracer) is usually needed; in the ocean it is most often a temperature contrast, while in the laboratory we use a dye. The images of the flow can be used to reconstruct the velocity field in the flow, most often by using the maximum cross-correlation method. In this method, the displacements of small regions of the patterns of the passive tracer are estimated between sequential images using cross correlations between small rectangular sections from each image. This is a technique that is widely used in experimental fluid dynamics.[3] When small particles of neutral density are seeded in the fluid to create the texture of the image this technique is called particle imaging velocimetry (PIV). In this experiment we use small (diameter=50 μm) plastic spheres of almost the same density as water to visualize the flow. Commercial PIV systems are usually very expensive. Quite accurate measurements, however, can be obtained using a personal computer equipped with suitable mathematical software (e.g., MATLAB[4]) and an inexpensive computer video camera. We used MATLAB code[5] to perform the analysis of the correlations. A complete description of the proposed experiment together with sample images and videos can be found at the author's web page.[6]

II. EXPERIMENT

The experimental apparatus is illustrated schematically in Fig. 2. The flows are generated in a Plexiglas™ tank of dimensions 25 cm×10 cm×10 cm. The sharp tip of an epidermic needle of internal diameter 0.05 cm is carefully cut off. This needle is then connected by plastic tubing to a burette with a stop-cock. Any 15- to 25-ml burette graduated in tenths of a milliliter can be used for this purpose. A PC video camera (USB version) is used to record the video sequences of the flow. This camera captures video and snapshots with VGA resolution (640×480 pixels). The video can be saved in AVI format, or alternatively, individual frames can be saved in common bitmap formats. Polyamid seeding particles (mean diameter 50 μm and density 1.03 g/cm^3) supplied by Dantec[7] are used for PIV measurements. The flow is illuminated either by a fluorescent lamp placed below the

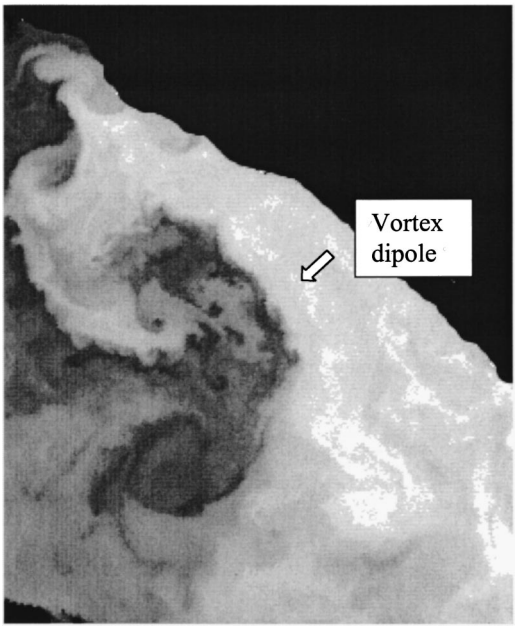

Fig. 1. Satellite image of the eastern Black Sea (Ref. 2). A vortex dipole is formed by cold water as shown by dark color.

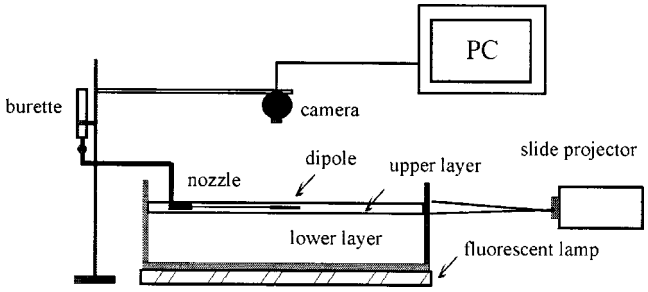

Fig. 2. Experimental setup.

tank, for the experiments with the flow visualized by dye, or by a slide projector placed at the side of the tank, for PIV measurements.

A general outline of the steps involved in the experiment follows.

A. Density stratification

The simplest case of stratification is a two-layer system. A Plexiglas tank is filled with two layers of fluid with differing densities. The lower layer can be relatively thick, 2–3 cm, and should consist of heavy fluid, such as salt water with a salt concentration of 50–100 g/l. The upper layer should be as thin as possible, 0.3–0.5 cm, and consist of a light fluid, such as fresh water. To prepare a two-layer system without mixing the fluids, one can float a sheet of paper on top of the salt water. The fresh water is carefully poured onto the sheet, and the latter is then (very carefully) removed.

B. Observation of vortex dipoles

The nozzle (epidermic needle) is placed horizontally in the upper layer. Fresh water that has been dyed by blue or black food dye is used to generate a horizontal jet flow from the nozzle. This submerged jet is used to produce the action of a localized force on the fluid. Figure 3 shows the development of the vortex dipole. By lowering and raising the burette, one can vary the difference Δh between the water level in the tank and that in the burette and thereby vary the intensity of the flow from the nozzle. The height of the burette is adjusted so that the flow is laminar. A movie of the developing flow is then recorded for 1 min using a video frame rate of 5 frames/s. The time required for the level of the water in the burette to fall at certain amount (e.g., 0.5 or 1.0 ml) is also measured during the experiment. Note that the level of water in the burette should not change too much since it is desirable to keep Δh almost constant so that the intensity of the flow from the nozzle is constant. The ratio of this volume to the measured time interval gives the mean volume flux q. The recorded video is then used for measuring the dimensions of the dipole (D and L in Fig. 3) at different times.

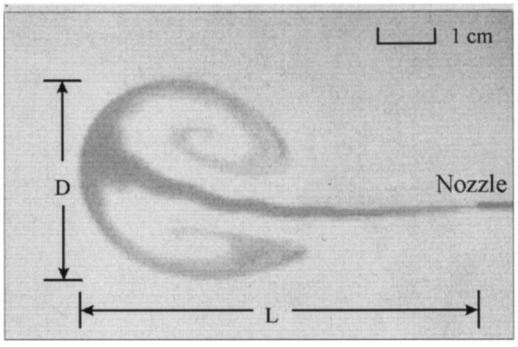

Fig. 3. Typical videoframe of the developing vortex dipole.

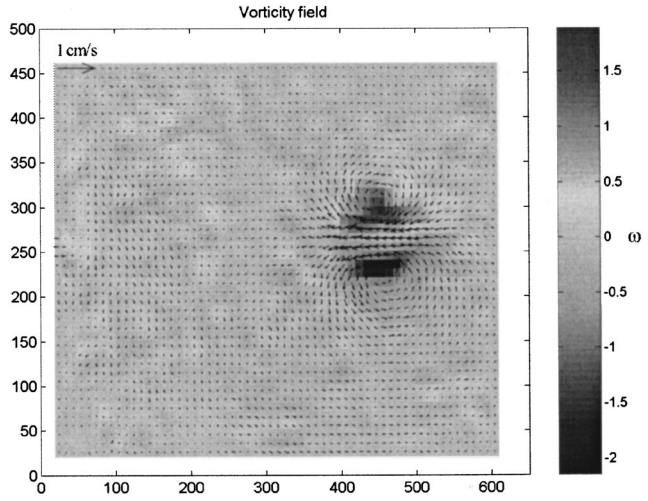

Fig. 4. Typical frame from a video of the flow with seeding particles.

C. Particle image velocimetry

In this part of the experiment, a new two-layer sample is prepared using salt water and fresh water, with the fresh water layer containing seeding particles. Fresh water, containing no particles or food dye, is used to generate a jet from the nozzle. A sheet of black paper is placed under the tank. The flow is illuminated from the side. (A slide projector is well suited to this purpose). Two strips of black paper are fixed to the side of the tank to create a slit so that only the interface between the two layers is illuminated. It is important to eliminate unwanted light so that neither the surface of water nor the bottom of the tank is illuminated. The developing flow was recorded in the same manner as above using a frame rate of 5 frames/s. A sample video frame is shown in Fig. 4.

III. DATA ANALYSIS

Using the camera software, individual frames from the recorded video of the flow of dye in the first experiment can be saved and then analyzed using the standard MS Windows image tool ''Paint.'' The position of the cursor in pixels is used to measure the length L and width D of the dipole (Fig. 3) at different frames. A centimeter scale placed under the tank prior to recording the video can be used to determine the resolution of the images (in pixels/cm) so that L and D can be calculated in centimeters. The dimensions of the dipole, namely L and D, are then plotted as functions of time. Dimensional analysis can be used to show that the time dependence of both L and D is given by $(\nu t)^{1/2}$ where ν (cm^2/s) is the kinematic viscosity (for water $\nu = 0.01$ cm^2/s). This implies that the flow is governed mainly by the viscous force, which is to say that L and D depend only on the coefficient of kinematic viscosity ν and time t. Previous studies[1] show that dipoles develop self-similarly, which implies that L is proportional to D, i.e., $L = \alpha D$, where the coefficient of proportionality α is a function of the Reynolds number (Re) of the flow. The coefficient α is plotted as a

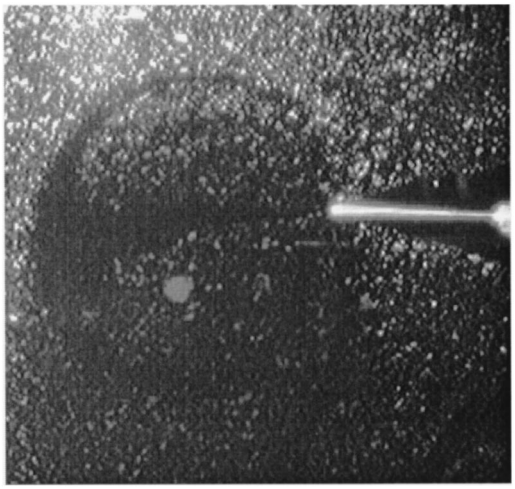

Fig. 5. The proportionality constant α for different values of the square of the Reynolds number.

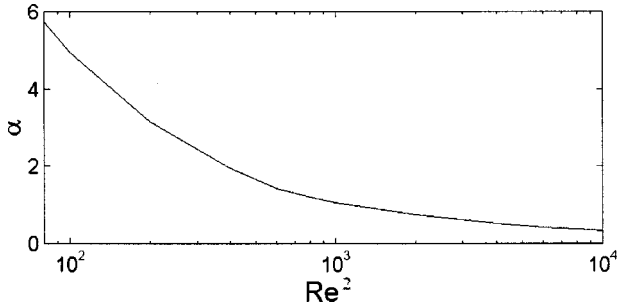

Fig. 6. Grayscale version of a typical colored vorticity map for the dipole obtained in the experiment. Vorticity in units of s^{-1}. Velocity field is shown by arrows. Distance is in pixels, 1 pixel = 0.034 cm.

function of Re^2 in Fig. 5. The curve in Fig. 5 represents the best fit to the data obtained in previous experiments.[1] The Reynolds number can be determined from α, which is typically about 2, corresponding to a Reynolds number of approximately 20. At this value of Re the flow is laminar and the dipoles are well formed.

The Reynolds number can also be estimated from the momentum flux from the nozzle. Consider a jet from a round nozzle of internal diameter d that is injected into surrounding fluid. If the mean velocity at the nozzle exit is U then the mass flux ρq is proportional to $q=\pi d^2U/4$. Here q is the volume flux measured in the experiment and $\rho=1$ g/cm^3 is the density of water. If a kinematic quantity J is defined as

$$J=\pi d^2U^2/4=4q^2/(\pi d^2),$$

then the momentum flux transported by the jet from the nozzle is given by the product ρJ. According to Newton's second law of motion, the rate of change of the momentum of the system is equal to the magnitude of the force applied. Thus the source acts on the fluid with a total force $F=\rho J$. It can also be shown[1] that the Reynolds number defined using the appropriate scales of the flow is related to J as $Re^2=J/\nu^2$. The value of Re that is calculated using this relation can then be compared with that obtained previously from the graph. The two values of Re typically correspond within 10%–20% accuracy.

Two consecutive frames from the video sequence of the experiment with the seeding particles are saved and then processed by the PIV software.[5] In this procedure a small subregion of an initial image is cross correlated with the same size subregion in a subsequent image, searching for the location in the second image which gives the maximum cross-correlation coefficient. This gives the displacement of the water parcel corresponding to this subregion and, knowing the time interval elapsed between the frames, the velocity of the parcel. A simple version of such a procedure can be easily programmed with just a few lines of MATLAB code. More advanced PIV *procedures* require interpolating velocity vectors to achieve subpixel resolution.[3] Our PIV software[5] calculates two components of velocity, V_x and V_y, and the vorticity field ω (Fig. 6) for each small subregion with coordinates (x, y). These quantities are represented by arrays in the MATLAB code. These arrays are kept in memory and can be used for further analysis. It is easy for students to write simple MATLAB commands in order to verify that the total vorticity in the flow is almost zero (a sum of all positive and negative elements of the array ω is small) and to estimate the x and y components of the total momentum of the flow (sums of the elements of the arrays V_x and V_y, respectively). This gives the momentum per unit height of the upper layer of fluid.

IV. CONCLUSION

We have presented a laboratory experiment to study vortex dipoles in a density stratified fluid using particle image velocimetry. Its principal pedagogical value is that it demonstrates how basic conservation laws can be applied to a complex fluid flow. Learning the main principles of the operation of the PIV system, in particular the analysis of the correlation between two patterns, exposes students to the kind of data processing that is often encountered in advanced research.

ACKNOWLEDGMENTS

This work was supported in part by the Natural Sciences and Engineering Research Council of Canada under Grant No. 227192-00. We are grateful to Dr. G. Pawlak for providing the software for the PIV and to Dr. C. Deacon for a thorough proofreading of the manuscript.

[a]Electronic mail: yakov@physics.mun.ca

[1]S. I. Voropayev and Ya. D. Afanasyev, *Vortex Structures in a Stratified Fluid: Order from Chaos* (Chapman and Hall, London, 1994).
[2]Ya. D. Afanasyev, A. G. Kostianoy, and A. G. Zatsepin, "Analysis of velocity field in the eastern Black Sea from satellite data during the 'Black Sea'99' experiment," J. Geophys. Res.-Oceans (submitted).
[3]A. M. Fincham and G. R. Spedding, "Low cost, high resolution DPIV for measurement of turbulent fluid flow," Exp. Fluids **23**, 449–462 (1997).
[4]http://www.mathworks.com
[5]G. Pawlak and L. Armi, "Vortex dynamics in a spatially accelerating shear layer," J. Fluid Mech. **376**, 1–35 (1998).
[6]http://www.physics.mun.ca/~yakov
[7]Dantec Dynamics. Polyamid Seeding Particles 38A2121 PSP-50.

Determination of melting temperature and heat of fusion of a solid using a computer-interfaced temperature probe

Mahantappa S. Jogad[a)]
Sharanabasaveshwar College of Science, Gulbarga-585 103, Karnataka, India and Department of Physics and Astronomy, Michigan State University, East Lansing, Michigan 48824-1321

David Van Domelen
Lyman Briggs School, Michigan State University, East Lansing, Michigan 48824

Gary Westfall, Walter Benenson, and S. D. Mahanti[b)]
Department of Physics and Astronomy, Michigan State University, East Lansing, Michigan 48824-1321

(Received 12 December 2000; accepted 10 August 2001)

This paper describes a relatively simple laboratory exercise enabling students to find the melting temperature of a solid with a low melting point, and to estimate its heat of fusion.
[DOI: 10.1119/1.1412722]

I. INTRODUCTION

The melting of solids is a topic of considerable general interest. A theoretical prediction of the melting temperature must take into account a large number of factors, including structures at many levels (atomic, molecular, and intermolecular), electric charges, bond strengths, and the size and mass of various atoms, etc. In addition, it involves the statistical mechanics of a many-particle system, thus making theoretical calculations of the melting point rather difficult.

Experimental determination of melting temperature is equally problematic. To get an accurate value for the melting point of a solid, one needs a pure sample, uniform heating, and a probe that does not interfere with the property it is measuring.

If the above conditions are met, as thermal energy is applied to a solid, its temperature will rise according to the following relationship:

$$Q = mc\Delta T, \tag{1}$$

where Q is the amount of energy absorbed, m is the mass of the solid, c is the specific heat of the object in J/(kg K), and ΔT is the change in temperature. Once the melting temperature is reached, the solid will continue to absorb energy, but its temperature will not rise until it has completely liquefied. Melting is the transformation from the solid state to the liquid state; it is an endothermic phenomenon. During this time, the change in energy will be equal to the heat of a fusion, H_f. The energy content of a liquid is always greater than that of a solid from which it forms. When a liquid freezes, energy is released to the surrounding. The amount of heat Q required to melt a solid is equal to heat released by the liquid when it freezes, therefore $Q = H_f$. Once the solid has liquefied completely, the temperature of the material will continue to rise in accordance with Eq. (1) but the specific heat capacity c is now that of the liquid.

In practice, pure samples are very difficult to obtain (especially pure samples that melt at temperatures safe for use in an undergraduate laboratory), perfectly even application of heat is almost impossible (even under research lab conditions), and no probe is completely noninterfering. As a result, the substance is likely to undergo a slight change in temperature as it melts, and the division between regular heating (before or after melting) and melting will not be particularly sharp. Additionally, while the temperature at which the solid becomes liquid (melting point) should be identical to the temperature at which the liquid becomes solid (freezing point), disorder in the atomic and molecular level (for example, in alloys) can cause the two to differ. A more detailed discussion of the current state of melting point measurements can be found in Refs. 1–3.

The lab exercise presented in this paper does not require pure samples, uniform heating, or a noninterfering probe, and should allow students to see results that demonstrate the general form of the melting curve.

II. EXPERIMENT

A. Apparatus

This laboratory exercise uses PASCO's Data Studio software and related hardware, including the PASCO signal interface (CI-6560) and two temperature probes (CI-6505A). One needs the following equipment: (1) hot plate heater; (2) Pyrex™ beakers, 100–259 ml; (3) ring stand and clamps to hold the temperature probe; (4) a known quantity of paraffin wax; and (5) safety goggles.

Prior to the class, the instructor should prepare the beakers by melting a known mass of wax in each beaker, making sure to label how much mass of wax is in each beaker. Insert the temperature probes into the beakers of molten wax, with the probe tips roughly halfway between the surface of the wax and the bottom of the beaker. Then allow the wax to cool. (Be careful to use a low heat setting while melting the wax, as it may boil at the bottom of the beaker if heated too rapidly, with unpleasant results.)

B. Setup

Place the beaker containing the desired sample on the hot plate, and then secure a temperature probe with a clamp mounted on a ring stand. The probe should firmly touch the surface of the wax, making a slight indentation. Plug the temperature probe into the signal interface, and select the probe in Data Studio. Set the probe to take data every second. Create a graph in Data Studio, with time along the horizontal axis and temperature along the vertical axis.

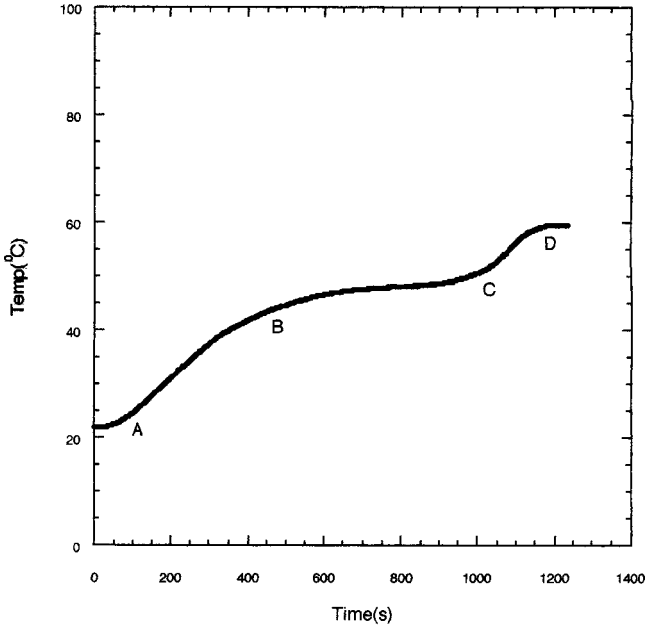

Fig. 1. Plot of temperature vs time for melting 50 g of paraffin wax on a hot plate at a setting of 3 (heating curve).

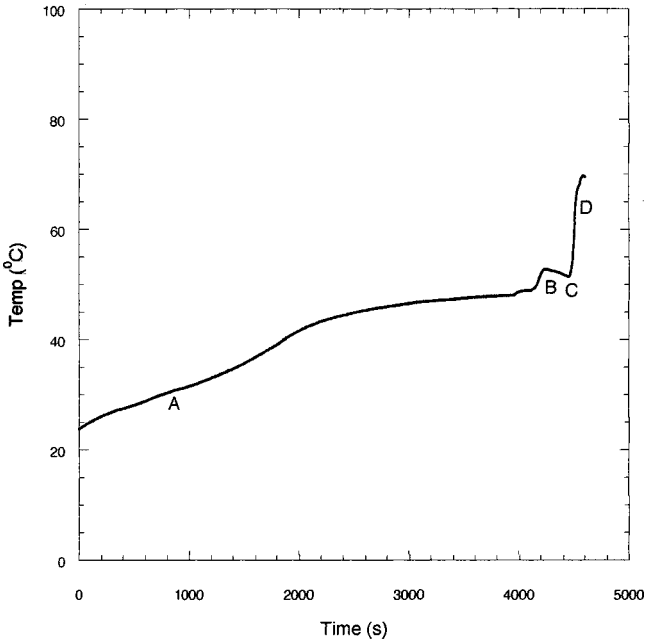

Fig. 2. Plot of temperature vs time for melting 10 g of paraffin wax on a hot plate at a setting of 3 (heating curve).

C. Procedure

1. Heating: (a) Turn the hot plate on to a low setting, roughly a third of the maximum. The instructor should perform the lab in advance to determine the optimum setting, but it is better to use a low setting and wait longer for the results than to use a high setting and have hot wax spit out. (b) After a few seconds, start collecting data as the sample heats slowly. As can be seen from the sample graph in Fig. 1, the heating process will take some time if the sample is large (over 20 g). It is a good idea to have an auxilliary exercise available to keep the students occupied during the 20–30 min of data collection. (c) Once the graph has started trending upwards again after a stretch of relative flatness, continue to take data until the temperature has increased by another 10° or so, then stop data collection and turn off the hot plate. (d) Using the cursor in Data Studio, determine the time and temperature for the following events: (*A*) the beginning of data collection, (*B*) roughly where the graph starts to almost flatten out, (*C*) roughly where the graph starts to rise again, (*D*) the end of data collection. Points *B* and *C* require some guessing, as there is not a sharp transition point (as seen in Fig. 1, for paraffin). The wax is undergoing a phase transition from solid to liquid between *B* and *C*. For a smaller sample, the graph may more closely resemble the one in Fig. 2; in which case points *B* and *C* are nearly the same.

2. Cooling: (a) Turn the hot plate on to a low setting, roughly a third of maximum. Take solid wax in a metal can (aluminum or any) and place on the hot plate. Heat until the wax is completely melted and heat a little bit more. Then take away the hot plate. (b) Transfer the metal can of melted (liquid wax) into a styrofoam cup containing 100 ml of water. After a few seconds, start collecting data as the sample cools slowly.

Place one temperature sensor inside the molten wax, and use the second temperature sensor to measure the temperature of the surrounding water bath. (c) Once the temperature graph has started trending downwards after a stretch of relative flatness, continue to take data until the temperature has gone down by 20° or so, then stop data collection. This is shown in Fig. 3 for wax cooling in a water bath. (d) Using the cursor in Data Studio, determine the time and temperature for the following events: (*A*) the beginning of data collection, (*B*) roughly where the graph starts to almost flatten out, (*C*) roughly where the graph starts to drop again, (*D*) the end of data collection.

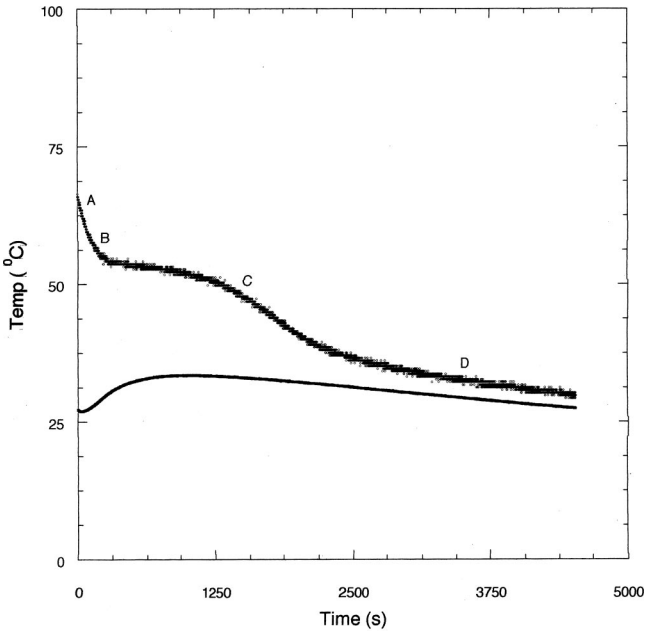

Fig. 3. Plot of temperature vs time for 50 g of paraffin wax cooling in a water bath (cooling curve). The upper curve represents the cooling of 50 g of wax. The lower curve shows the temperature of the 100-ml water bath.

III. ANALYSIS

1. Melting (fusing) temperature and rate of heat absorption (loss) by the wax. First, students should find the approximate melting point of the wax. Taking the temperatures at points *B* and *C* of Fig. 3 and averaging them can do this. Compare this result to the accepted value between 52 and 60 °C for most commonly available paraffin. For small samples, there may not be a flat region during which the phase transition occurs; the transition may take place fairly abruptly, over the course of only a few seconds, as seen in Fig. 2. In that case students should examine the graph for a sharp ''kink'' in the line, where the heating curve shifts between the solid and liquid phases. Next, students can estimate the rate at which thermal energy is absorbed by the solid wax and the liquid wax while heating.

Equation (1) can be used to calculate the energy absorbed Q_s, by the solid wax between points *A* and point *B* (see Fig. 1), using that the specific heat of wax is approximately 0.69 cal/g °C.[4,5] Dividing this value of Q by the time interval Δt_{AB} between points *A* and *B*, one can estimate the average rate of energy absorption by the solid wax, $Q_s/\Delta t_{AB}$.

Similarly, one can determine the energy absorbed between points *C* and *D* (see Fig. 1) Q_1, assuming that the specific heat of liquid wax is the same as that of the solid. Divide this value of Q_1 by the time interval Δt_{CD} between *C* and *D* to get the average rate of energy absorption by the liquid wax, $Q_1/\Delta t_{CD}$.

2. Estimating the heat of fusion. To estimate the heat of fusion, H_f, one can assume that the rate at which thermal energy is taken away from the wax during the melting (where solid and liquid coexist) is the average of the cooling rate of the solid and the cooling rate of the liquid.

Taking the average of $Q_1/\Delta t_{AB}=1.725$ cal/s and $Q_s/\Delta t=0.299$ cal/s and the time interval between *B* and *C* ($\Delta t_{BC}=1517$ s), from Fig. 3 one can estimate the heat of fusion H_f. The product of the time interval between *B* and *C* ($\Delta t_{BC}=1517$ s) and the average of liquid cooling and solid cooling rates gives total $Q=1535$ cal. Since the mass of the paraffin wax is 50 g, the heat of fusion per gram is 30.7 cal/g. This value agrees well with the measurements $H_f=25-42$ cal/g quoted in Refs. 3, 5, and 6 for different commercial waxes.

Similarly, from the heating graph (see Fig. 1) taking the average of $Q_s/\Delta t_{AB}=1.861$ cal/s and $Q_1/\Delta t_{CD}=2.024$ cal/s and the time interval between *B* and *C* ($\Delta t_{BC}=548.3$ s), from Fig. 1 one can estimate the heat of fusion H_f. The product of the time interval between *B* and *C* ($\Delta t_{BC}=548.3$ s) and the average of solid cooling rate and liquid cooling rate gives total $Q=1065$ cal for 50 g. Thus, the heat of fusion of paraffin wax $=21$ cal/g. This value lies somewhat below the values $H_f=25$ cal/g-42 cal/g quoted in Refs. 3, 5, and 6 for different commercial waxes.

IV. CONCLUSION

In summary, we have presented a simple experiment to measure the melting temperature and heat of fusion of a solid. This lab can be performed with any solid that melts between room temperature and the boiling point of water, although it is recommended that one use only low melting temperature substances for safety reasons. Different types of wax such as beeswax and carnauba wax with different melting points and specific heats may also be substituted.

It might also be useful to give different amounts of wax to each student group, so that some get graphs like Fig. 1 and others get graphs like Fig. 2. Then the class as a whole can discuss these differences.

ACKNOWLEDGMENTS

One of the authors, MSJ, is thankful to the American Physical Society Kilambi Ramavataram (APS-KR) Committee, the Fulbright Foreign Scholarship Board, the Michigan State University, East Lansing, and the University of Nebraska Lincoln for their financial support. He is also thankful to Dr N. Anantaraman, chairperson, American Physical Society Kilambi Ramavataram.

[a]Electronic mail: mahjogad@rediffmail.com
[b]Electronic mail: mahanti@pa.msu.edu

[1]D. S. Barnby, L. G. Bostwick, and J. A. Huston, Jr., ''Some Studies on the Physics of Paraffin Wax and Wax/Polymer Systems,'' Proceedings of the Sixth World Petroleum Congress **6**, 161–178 (1963).
[2]Mahantappa S. Jogad, Ph.D. thesis, Gulbarga University, Gulbarga, India, 1998.
[3]M. G. Broadhurst, ''An Analysis of the Solid Phase Behavior of the Normal Paraffins,'' J. Res. Natl. Bur. Stand., Sect. A **66A**, 241–249 (1962).
[4]*Concise Encyclopedia of Science and Technology* (McGraw–Hill, New York, 1984), p. 58.
[5]J. M. Power, R. G. Craig, and F. A. Peyton, ''Calorimetric analysis of commercial and dental waxes,'' J. Dent. Res. **48** (6), 1165–1170 (1969).
[6]David R. Lide, *CRC Handbook of Chemistry and Physics* (CRC Press, Boca Raton, FL, 1995–96), 76th ed.

A simple demonstration of Mie scattering using an overhead projector

Charles L. Adler[a)]
Physics Department, St. Mary's College of Maryland, St. Mary's City, Maryland 20686

James A. Lock
Physics Department, Cleveland State University, Cleveland, Ohio 44115

(Received 16 May 2001; accepted 15 August 2001)

[DOI: 10.1119/1.1412647]

Light scattering by small particles is a complicated and sometimes counterintuitive subject. In particular, the dependence of the scattering cross section on wavelength of light can be quite different for different particle sizes. For example, Rayleigh scattering by particles that are small compared to the wavelength is responsible for the red sunset and blue sky, while scattering by larger particles can lead to the opposite effect: the so-called ''blue moon'' or ''green sun''

occasionally seen after forest fires or volcanic explosions.[1] Straightforward classroom demonstrations of light scattering exist: The Rayleigh scattering regime can be created by using a dilute suspension of milk in water, while demonstrations involving larger particles can be created using cigarette smoke.[1,2] However, the problem with both of these methods is that one cannot effectively control the size (or shape) of the scatterers, or even say much about the distribution of particle sizes.

A simple demonstration of the particle-size dependence of Mie scattering can be performed using an overhead projector and two suspensions of polystyrene microspheres: one with 500-nm-diam particles and the other with 1740-nm-diam particles. Suspensions of polystyrene microspheres are widely available; the particles are almost perfectly spherical, and the particle radii vary by no more than about $\pm 1\%$ in a typical suspension. The range of available sizes is also quite large; one can purchase suspensions with mean particle size from under 100 nm to greater than 100 μm. The refractive index of the particles is about 1.59 in the visible region of the spectrum, leading to a relative refractive index of 1.19 when the particles are suspended in water.

For the demonstration, an overhead projector is set up with a transparent tray on the platen. (A clear plastic plate, like the kind used for picnic lunches, is ideal.) The tray is filled with water to a depth of 2 or 3 mm, and the image of the tray is projected onto a screen, as shown in Fig. 1. The 500-nm-diam scatterers are now mixed in with the water, and the image on the screen turns a brownish-red! To make the demonstration more dramatic, the micropsheres should be dripped into the water directly from their original plastic squeeze bottle. The bottle can be passed around to the students before or after the demonstration to show that the particles are not colored in any way. After this, a new tray is placed on the overhead and the 1740-nm-diam particles are dripped into the water. This time, the image turns a vivid, dark blue!

Here's what's happening: Some of the light from the overhead lamp that passes through the suspension is scattered by the polystyrene microspheres. The scattered light misses the imaging optics of the overhead. (For a description of how an overhead projector works, see Goodman's wonderful little book.[2]) However, the scattering cross section of the particles is strongly wavelength dependent. For transparent spheres with relative index of refraction close to 1, the scattering cross section can be approximated by[3]

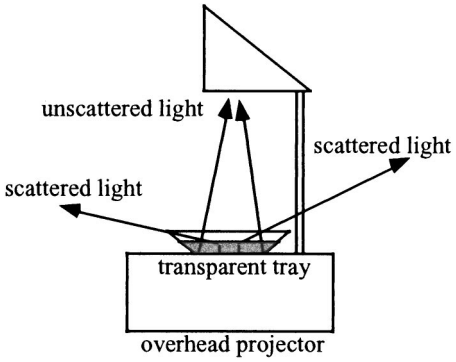

Fig. 1. Demonstration setup. In our demonstrations, the tray is a small, transparent plastic plate.

$$Q = 2 - \frac{4}{\rho}\sin\rho + \frac{4}{\rho^2}(1-\cos\rho), \tag{1}$$

where $Q = C_{\text{scat}}/\pi a^2$, C_{scat} is the scattering cross section, a is the particle radius (250 and 870 nm, respectively), and $\rho = 4\pi(m-1)na/\lambda$. Here, $m = 1.19$ is the relative index of refraction, $n = 1.33$ is the index of the medium surrounding the particles, and λ is the wavelength of the incident light in air. In the words of van de Hulst, "this is one of the most useful formulae in the whole domain of Mie scattering, because it describes the salient features of the extinction curve not only for values of m close to 1, but even for values of m as large as 2."[3]

Figure 2 shows a graph of Q vs ρ for $n = 1.33$ and $m = 1.19$. We show both the exact Mie theory cross section and the approximation of Eq. (1). The chief differences between the two are that Eq. (1) underestimates Q by about 20% for the values of ρ examined here, and does not have the high-frequency ripple for large values of ρ. As is seen, Q is an oscillatory function of ρ. For fixed particle radius, increasing ρ implies decreasing wavelength, while for fixed wavelength, ρ increases as the particle size increases. For large ρ, Q approaches 2, meaning that for particles very large compared to the wavelength, the scattering cross section approaches $2\pi a^2$.[3] Several regions of the extinction curve are boxed in Fig. 2. The boxes enclose the region of the scattering curve for visible wavelengths of light (400–700 nm) for four different particle diameters. Region (a) represents the cross section for light scattering by particles with a fixed diameter of 500 nm, and region (b), a fixed diameter of 1740 nm. Note that for region (a), the center of the scattering region in Fig. 2 is approximately at the point where the slope of the extinction curve is greatest, implying the greatest difference in the scattering cross section for blue and red light. Because the cross section is greater for shorter wavelengths than for longer wavelengths, the image of the suspension will appear red, as more blue light is scattered out of the system than red. It should be noted that the wavelength dependence of the

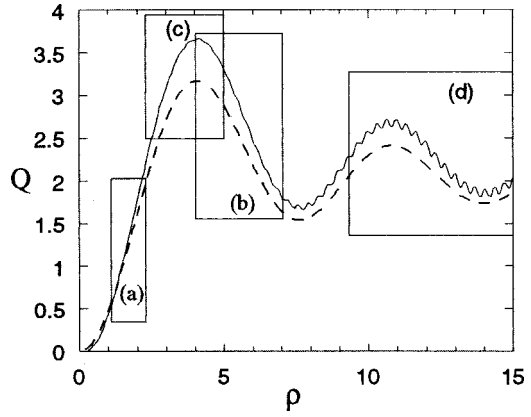

Fig. 2. Scattering cross section (Q) as a function of size parameter (ρ). The dashed line was calculated using Eq. (1), which is valid for small m, while the solid line was calculated using Mie theory. The boxes on the graph enclose the scattering curve for wavelengths in the visible region of the spectrum for the following particle diameters: (a) scattering cross section for 500-nm-diam particles as a function of ρ; (b) scattering cross section for 1740-nm-diam particles as a function of ρ; (c) scattering cross section for 1000-nm-diam particles as a function of ρ; (d) scattering cross section for 4000-nm-diam particles as a function of ρ. The entire scattering region for this particle size extends slightly beyond the end of the graph (to $\rho = 15.8$).

scattering cross section for the smaller particles cannot be explained by Rayleigh scattering.[3] Rayleigh scattering is only valid for particle radii small compared to the wavelength, which is not true here.

The situation is reversed for the 1740-nm-diam particles. Here, the center of region (b) in Fig. 2 lies where the slope of the extinction curve is near its minimum value (i.e., strongly negative). This means that the scattering cross section is greater for longer wavelengths, leading to the blue image. Note that the two particle sizes were chosen so that the *slope* of the scattering curve would be extremal, not the scattering curve itself.

The scattering region for particles with a diameter of 1000 nm for visible light is shown in box (c) of Fig. 2. Here, the center of the scattering curve lies near the maximum value of Q. This means that the image should be essentially uncolored, as the scattering cross section is almost the same for visible wavelengths. Doing the demonstration using these particles confirms this—no coloration of the image is seen.

One can perform similar demonstrations using larger particles. However, there is a complication: For larger particles, the range of ρ values corresponding to visible wavelengths increases as the particle diameter increases. This can be seen by comparing the two regions for the 500- and 1740-nm-diam particles: The range of ρ values is over three times as large for the larger particles as it is for the smaller ones. Could one use this to choose a particle size where both red and blue light were strongly scattered, leading to an image which was colored yellow or green? The range of ρ values for a 4000-nm-diam particle lies between about 9.1 and 15.8; this extends from just before one maximum in the scattering cross section to near the next maximum, implying that intermediate wavelength light (yellow and green) should be scattered least, and long- and short-wavelength light scattered most. Part of the scattering region is enclosed by box (d) in Fig. 2, although it extends beyond the end of the graph. We have performed this experiment: The resulting image looks dark grayish green. It may be possible to make the coloration more vivid by a better choice of particle size (4300-nm-diam particles would probably work better), but we have not tried this yet. If any readers make the attempt, we would be very interested in learning the results of their work.

The one drawback with this demonstration is the relatively high cost of polystyrene microspheres—roughly $200 for a 15-ml bottle. One bottle is good for at least 20 demonstrations, however, which is probably good for a few years. (Our bottles are usually depleted because we do this demonstration quite often!) One can mix the suspensions ahead of time so that they can be used again, although this robs the demonstration of a good deal of drama. Finally, if any readers are interested in images we have made from the scattering demonstrations listed here, they can contact the authors.

[a)]Electronic mail: cladler@osprey.smcm.edu.

[1]Craig Bohren, *Clouds in a Glass of Beer* (Wiley, New York, 1987), pp. 91–97.

[2]Douglas S. Goodman, *Optics Demonstrations on the Overhead Projector* (Optical Society of America, Washington, DC, 2000), p. S-6.

[3]H. C. van de Hulst, *Light Scattering by Small Particles* (Wiley, New York, 1957), pp. 176–178.

GORDON CONFERENCE ON PHYSICS RESEARCH AND EDUCATION: QUANTUM MECHANICS

The 2002 Gordon Conference on Physics Research and Education will focus on quantum mechanics and will be held on June 9–14, 2002 at Mount Holyoke College, South Hadley, Massachusetts. The goal of the conference is to bring together researchers who study and apply quantum mechanics, physics education researchers, and college and university level instructors of quantum mechanics for the purpose of promoting innovation in all aspects of teaching quantum mechanics throughout the undergraduate curriculum. The conference will include sessions and discussions about the desired content and outcome of courses, curriculum development using research on student understanding of topics in quantum mechanics, ways of approaching non-intuitive aspects of quantum theory, and the results of current research in physics that can be used to increase undergraduate student understanding of the concepts and applications of quantum mechanics. More information can be found at http://www.grc.uri.edu/programs/2002/physres.htm. Questions or suggestions about the Gordon Conference can be addressed to the organizers, Beth Ann Thacker (batcam@spudhammer.phys.ttu.edu), Harvey Leff (hsleff@csupomona.edu), or David Jackson (jacksond@dickinson.edu).